Meccanica (2012) 47:639–654
DOI 10.1007/s11012-011-9472-7

The effect of oil pressure and temperature on barrel film thickness and barrel dynamics of an axial piston pump

J.M. Bergada · D.L. Davies · S. Kumar · J. Watton

Received: 1 December 2010 / Accepted: 3 August 2011 / Published online: 6 September 2011

Abstract Efficiency improvement in piston pumps and motors is a major task in pump development. Just a small improvement in efficiency can have a significant financial impact, particularly on large manufacturing plants employing many large-power pumps. According to the bibliography, effort has been concentrated in studding slipper swash plate leakage, forces, torques and slipper dynamics, but less attention has been given to the understanding the barrel dynamics and the inherent clearance between the barrel and the port plate. This paper clarifies the understanding of the complex barrel dynamics, pointing out how barrel-port plate film thickness depends on oil pressure and temperature. The paper demonstrates that mixed lubrication exist between the barrel face and the port plate under some of the conditions studied, proving that elastic metal to metal forces play an important role when studding barrel dynamics. According to the authors, more effort should be considered into properly designing the barrel sliding surface since both volumetric and mechanical efficiencies are very much dependent on this design. Fluid used hydraulic oil ISO 32.

Keywords Axial piston pumps · Barrel dynamics

J.M. Bergada (✉) · S. Kumar
Fluid Mechanics Department, ETSEIAT UPC, Colon 11, Terrassa 08222, Spain
e-mail: bergada@mf.upc.edu

S. Kumar
e-mail: kumarsush@gmail.com

D.L. Davies · J. Watton
Cardiff School of Engineering, Cardiff University, Queen's Buildings, The parade, Cardiff CF24 3AA, Wales, UK

D.L. Davies
e-mail: daviesdll@cardiff.ac.uk

J. Watton
e-mail: wattonj@cardiff.ac.uk

Nomenclature

A_0	metal to metal contact area between the barrel and the port plate (m^2)
B	barrel damping coefficient (Nm/rad s^{-1})
E	Young modulus (N/m^2)
F_{forces}	torque created due to friction (Nm)
h_o	barrel-port plate central clearance (m)
I	barrel moment of inertia, versus a generic angle ($kg\,m^2$)
K	spring torsional constant acting over the barrel (Nm)
L_0	port plate width (m)
M_{EF}	elastic metal to metal torque (Nm)
M_E	elastic metal to metal torque constant (Nm)
M_X	fluid generated torque versus the barrel X axis (Nm)
M_Y	fluid generated torque versus the barrel Y axis (Nm)
p_{ext}	pump inlet (tank) pressure (N/m^2)
p_{int}	pump outlet pressure (N/m^2)
r	barrel central radius (m)
r_{int}	internal radius of the main groove (m)

r_{ext}	external radius of the main groove (m)
r_{int2}	internal land inner radius (m)
r_{ext2}	external land outer radius (m)
r_{mext}	external land average radius, between r_{ext} and r_{ext2} (m)
r_{mint}	internal land average radius, between r_{int} and r_{int2} (m)
R_{int}	internal radius of the timing groove (m)
R_{ext}	external radius of the timing groove (m)
R_{mint}	timing groove internal land average radius, between r_{int2} and R_{int} (m)
R_{mext}	timing groove external land average radius, between r_{ext2} and R_{ext} (m)
r_m; R_m	average radius between land borders (m)
α	barrel maximum tilt angle (rad)
η	barrel tilt angle perpendicular to Y axis (rad)
η_0	barrel initial angular position, perpendicular to Y axis (rad)
η_L	maximum barrel tilt angle perpendicular to Y axis for a given working conditions (rad)
δ	barrel tilt angle perpendicular to X axis (rad)
δ_0	barrel initial angular position, perpendicular to X axis (rad)
δ_L	maximum barrel tilt angle perpendicular to X axis for a given working conditions (rad)
ΔL	decrease in length due to compression forces (m)
γ	timing groove angle (rad)
μ	fluid dynamic viscosity (Kg/(m s))
θ	barrel main groove angle, versus the maximum tilt axis (rad)
ω	barrel angular velocity (rad/s)

1 Introduction

Axial piston pumps barrels, experience small oscillations due to the forces acting over them. Cavitation also occurs in many cases, sometimes damaging the plate and barrel sliding surfaces and therefore reducing the overall efficiency of the pump. Nowadays must also be considered that, the resulting failure of the pump is often a critical issue in modern industrial applications. The barrel complex fluctuation will be in the present work experimentally evaluated and the clearance between barrel plate and port plate will be analyzed. The present paper demonstrates the importance of properly designing the barrel-plate sliding surface, since pump efficiency is highly dependent on it. Some of the most relevant research related to piston pump barrel dynamics and leakage barrel-plate are next outlined.

From all the studies undertook in the past nearly 40 years, it can be stated that the performance of silencing grooves used in axial piston pumps barrel-port plate sliding surfaces and considering their effect on pressure ripple, leakage, noise generation, dynamic forces and torques acting over the barrel-port plate, was studied among others by [1–10]. The clearance and leakage between the barrel and port plate has been studied experimentally by [11–14], analytical research in this area has been presented in [5, 14–24], particularly innovative CFD research which included pressure distribution, thermal effects and the effect of micro structured wave surface in the barrel-port plate sliding surface has been undertaken by [25–29]. The piston pressure-flow dynamics was presented in [4, 22, 30–37], torques and forces acting on the swash plate were studied in [10, 21, 32–35, 38–43], friction barrel plate was analysed by [12, 26, 29, 44, 45]. Despite the amount of papers published on axial piston pumps and the huge knowledge gathered, it appears there is still further research to be done in order to better understand the barrel-port plate film thickness and the barrel dynamics associated. This paper considers these issues with the intention of establishing more detailed experimental data and validation of design equations that may be used to improve axial piston pumps overall efficiency.

2 Experimental test rig and measuring procedure

Figures 1 and 2 present the pump used for the experimentation; it is a nine piston axial design being its maximum volumetric displacement of 24.1 cc/rev and giving a maximum flow of about 35 l/min at its maximum swash plate angle of 20°. Figure 1(a) presents the pump internal view, in Fig. 1(b) it is seen the pump external view and the position of the transducers used, Fig. 1(c) presents the pump cross section where two of the three position transducers used to perform the measurements are to be seen. Pump axis, pump spring, swash plate and the bearings located at both axis ends are also presented in Fig. 1(c). Figure 1(d) defines the axes used to measure the exact position of the transducers presented in Fig. 1(b), also the pump rotational speed direction is given in the same Fig. 1(d). The

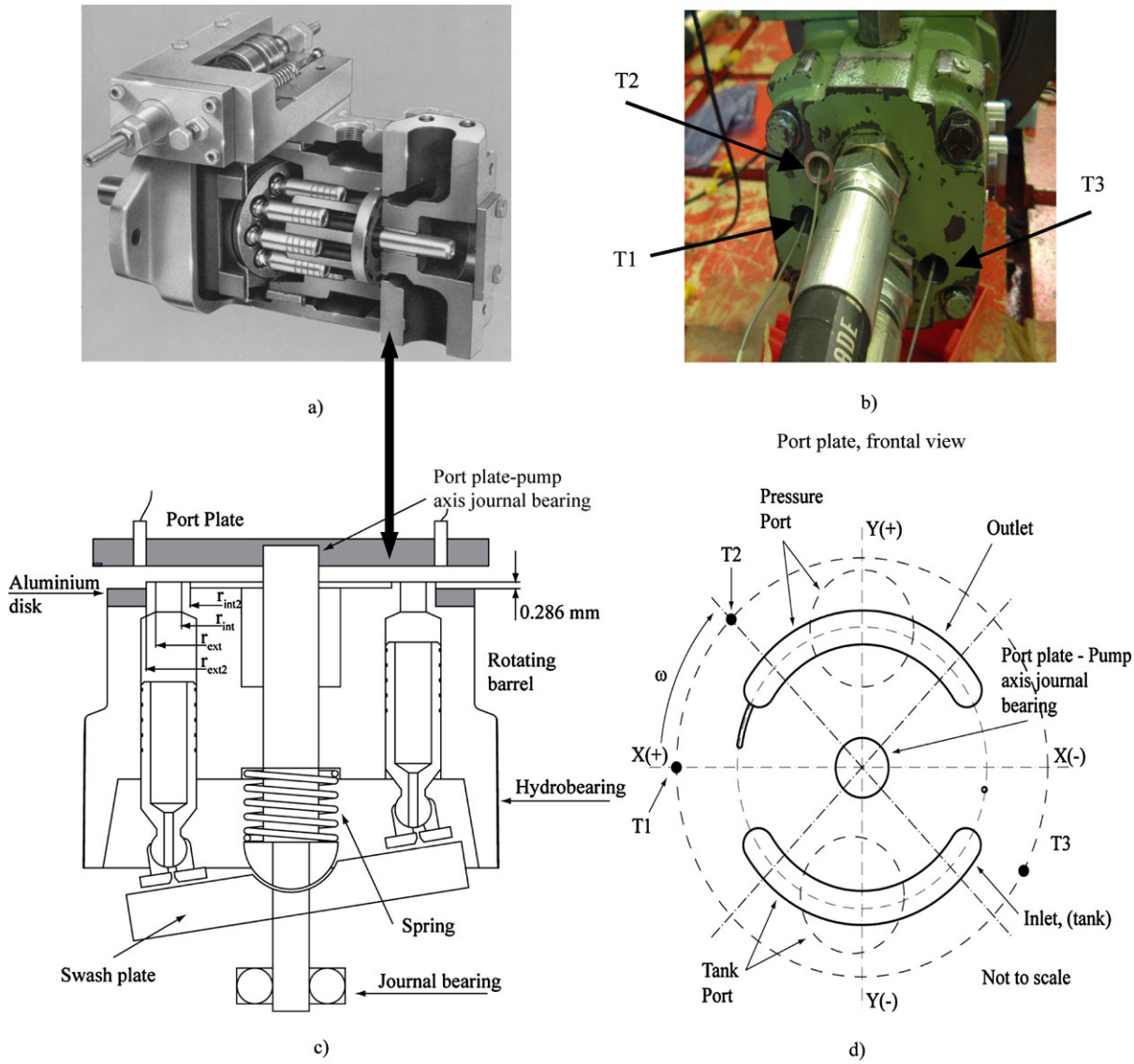

Fig. 1 Pump under study and location of the three displacement transducers

lower dash circle presented in this figure represents the pump inlet, the upper one represents the pump outlet and the big central one is approximately the diameter where the position transducers were located. On the pump port plate, Fig. 1(b), three Micro-Epsilon unshielded inductive position transducers, model NCDT 3010 were allocated, the maximum measuring range for each transducer was of 0.5 mm and each of them was capable of measuring to an accuracy of 0.1 μm. Such transducers offer a unique thermal stability of 0.05% FSO, being its temperature operation range of −50 to 150°C. The exact position of the transducers related to the XY axis represented in Fig. 1(d) was:

Transducer 1: $X_1 = 47.96$ mm, $Y_1 = 0.285$ mm

Transducer 2: $X_2 = 33.68$ mm

$Y_2 = 34.155$ mm

Transducer 3: $X_3 = -39.93$ mm

$Y_3 = -27.34$ mm

The transducers were calibrated one by one in a specific calibration test rig. Transducer's calibration

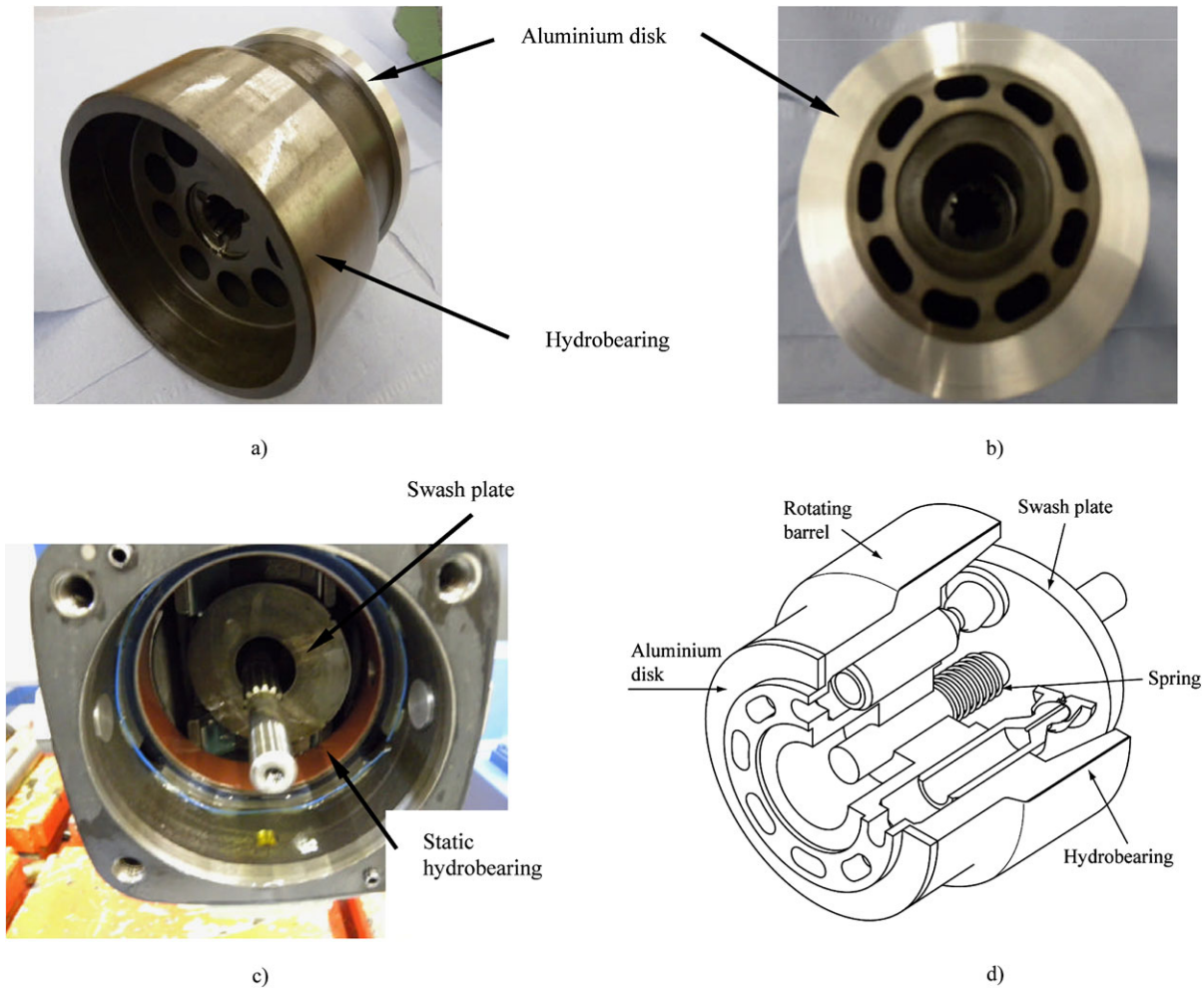

Fig. 2 Pump under study internal view

showed an excellent linearity, the calibration equation of each transducer being:

$$\text{Transducer 1;} \quad d_1 = 0.0487399V + 0.0296410 \text{ mm}$$

$$\text{Transducer 2;} \quad d_2 = 0.0452037V + 0.0328352 \text{ mm}$$

$$\text{Transducer 3;} \quad d_3 = 0.0476972V + 0.0322051 \text{ mm}$$

where V is the measured voltage [V] and d_i is the distance [mm].

After being calibrated, the transducers were screwed into the fixed port plate and facing the inner part of the pump, the rotating barrel. To find the transducers zero position, the port plate with the transducers inserted in it was placed over an aluminium plate perfectly flat, the readings given by the transducers when facing such plate gave the transducers zero position. Once having done it, the next step was to fix the port plate to the pump. Due to the preferred operation of each transducer, which needs to point at a non magnetic material, a thin aluminium plate was bonded to the barrel end, as shown in Figs. 1(c), 2(a) and 2(b). In order to show more precisely the modifications made on the barrel, Fig. 2 has been introduced. Figure 2(a) presents the axial piston pump barrel with the aluminium ring inserted on it. Figure 2(b) shows the frontal view of the aluminium disk used. Figure 2(c) presents the pump internal view, where the pump axis, swash plate and the so called by the manufacturer, hydrobearing, used to maintain the barrel aligned with the pump axis, are to be seen. It is to be noticed that the barrel external diameter turns

around the static hydrobearing fixed to the pump case; the clearance between them is, according to the manufacturer of around 10 μm being the static hydrobearing part, made of a plastic material similar to PTFE. Such a pump design, assures that once the barrel is inserted into the pump, the barrel can only be tilted a fraction of a degree versus its central position. Figure 2(d) introduces a three dimensional view of the barrel, where the barrel spring, aluminium disk and barrel hydrobearing are to be seen. The barrel and port plate are made of cast iron and the sliding surfaces are carbonitrided to a typical depth of 10 μm. The sliding surfaces roughness is of 0.4Ra.

The static run-out of the aluminium plate was of 7 microns, the average distance between the barrel face and the aluminium disk being 0.286 mm as indicated in Fig. 1(c). Two sets of test were undertaken, at swash plate angles of 10° and 20°, and for each case two oil temperatures 28°C and 45°C were studied. At each test, measurements were taken at pressures of 2.5, 5, 7.5, 10, 12.5, 15, 17.5, 19.5 MPa. Since the pump used has a pressure compensating unit, the maximum available pressure for the tests performed at 10 degrees swash plate angle and 45°C oil temperatures was 15 MPa. The measurements presented in the following sections, shows that the barrel position fluctuates, being the fluctuation highly dependent on pump inlet pressure and oil temperature. For the purpose of performance analysis the temporal barrel position and the barrel-plate oil film thickness will be expressed as a temporal average. The fluid used to perform the experiments was hydraulic oil ISO 32, being its main physical characteristics fully defined in the ISO standards.

3 Results

The measurements are divided into three parts; first some typical main sine waves measured by transducers T1, T2 and T3 will be presented, then, it will be introduced, the average distance between the port plate and the barrel aluminium disk, and finally analysis will be concentrated into understanding a second and much smaller amplitude fluctuation wave, which is sitting on the top of the main wave.

3.1 Main wave measured by the transducers

Figure 3, presents some measured results for the three transducers and for a pump outlet pressure of 10 MPa.

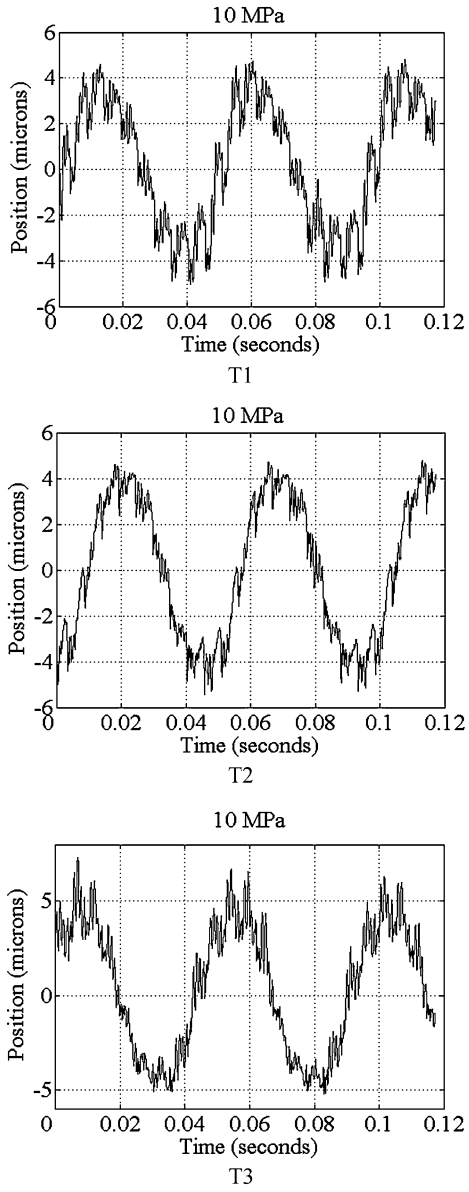

Fig. 3 Position fluctuation measured from transducers T1, T2, T3. Pump pressure 10 MPa. 20° swash plate angle and 45°C

This figure just presents the dynamic wave amplitude versus its central (x) axis, without considering the transducers zero positioning. The first think to notice is that there is a main sine wave and some fluctuations sitting on the top of it, which will be called the fluctuation wave. The main wave sine wave frequency, when considering the pump rotational speed of 1440 rpm is 24 Hz, the oscillation period being of 0.0416 seconds. This period is of course fixed for all the tests undertaken. The wave peak-to-peak amplitude is mostly due

to the barrel run out, which was measured to be 7 microns. It has to be noticed nevertheless, that the peak-to-peak found during experimentation was not constant and varied between 7 and 12 microns, depending on the pressure and the position of the transducer. An analysis of these variations is necessary; both for the main wave and the fluctuation wave, the present paper will focus on the fluctuation wave. Recall that transducer 1 always gives the maximum fluctuation wave amplitude.

3.2 Average distance between the port plate/barrel aluminium disc

Since the rotating aluminium measuring face has a run-out of 7 microns, the barrel/plate gap distance measured is changing over time. Therefore, the average distance is determined from a minimum of 20000 measurements for each position transducer location after taken into account each transducers initial position. It will be noticed that at some points, the average distances are smaller than the real average distance between the barrel face and the barrel aluminium disk, which is of 0.286 mm. This is due to the transducers being located outside the barrel sliding surface external diameter, see Fig. 1, where the tilt effect is more clearly noticeable. Also the pump plate has some small erosion due to metal-to-metal contact between the barrel and the plate and this erosion varies between 0 and 4 microns. A photograph of the plate inside face is presented in Fig. 4, showing several surface roughness graphs measured at different points located around port plate surface. Notice that erosion of around 4 microns is found in the area located between 45° and 225° anticlockwise from the position of transducer 1 shown in Fig. 4, in particular in positions 4 to 8. This clearly indicates that plastic metal to metal contact has occurred in this area. Similar erosion to the one presented in Fig. 4 was also found in the barrel sliding surface.

Figure 5 presents a typical graph showing the dynamic distance variation between the barrel aluminium disk and port plate, as measured by the three position transducers. The 7 micron peak-to-peak fluctuation can clearly be seen, although this value is not constant and varies for each transducer and with pump output pressure and oil temperature. It is necessary to consider that the barrel aluminium plate has a static run-out of 7 microns and therefore, the main wave amplitude is mostly due to the barrel dynamic run-out. It is relevant to point out that transducer 1 always gives the minimum barrel/port plate distance, transducer 2 gives the maximum distance, and more clearly at high temperatures. Transducer 3 presents a distance which is smaller than transducer 2, but the phase given by transducer 3 is displaced about 180° with respect to the phase presented by transducer 2. Since transducers 2 and 3 are respectively on the upper and lower part of the plate, and separated nearly 180°, such phase difference had to be expected. Transducers 1 and 2, have nearly the same phase, since they are close to each other. In most of the cases studied, the main wave amplitude from transducers 2 and 3, was bigger than the one given by transducer 1, indicating that a barrel oscillation exist about the X axis.

As a result of the previous explanation, the barrel position and film thickness need to be studied as a temporal average. From Fig. 5, it is also noticed, especially at high pressures, that a second fluctuation appears superimposed on the first one. This second fluctuation has been called in the previous section, the fluctuation wave, and it is directly related with the barrel vibration frequencies. Such a fluctuation is more relevant from transducer 1 and especially at high pressures and high temperatures, indicating that the torque fluctuation origin has to be along the X axis. Figure 5 shows that the average distance between the barrel aluminium plate and the port plate tends to slightly decrease as pressure increases.

In Fig. 6 the measured average distance between the barrel aluminium plate and port plate is shown as a function of pressure, temperature and swash plate angle. It is clearly noticed that as pressure increases, the average distance slightly decreases and therefore the average film thickness will be decreasing with pressure. It is also noticed that such a decrease is less than 12 microns and is higher at 20° swash plate angle than at 10° degrees swash plate angle. When comparing Figs. 6a, b, it is noticeable that at high temperatures, the film thickness decrease with pressure increase, is slightly higher (about 6 microns) than at low temperatures, yet the film thickness is considerably higher at low temperatures than at high ones. These results indicate that the maximum average film thickness is in general to be found around the axis position Y^+, then transducer 2 always gives the higher value.

Figure 4 demonstrates that around the area where transducer 2 is located, the metal-to-metal contact is not very significant since the surface is slightly eroded.

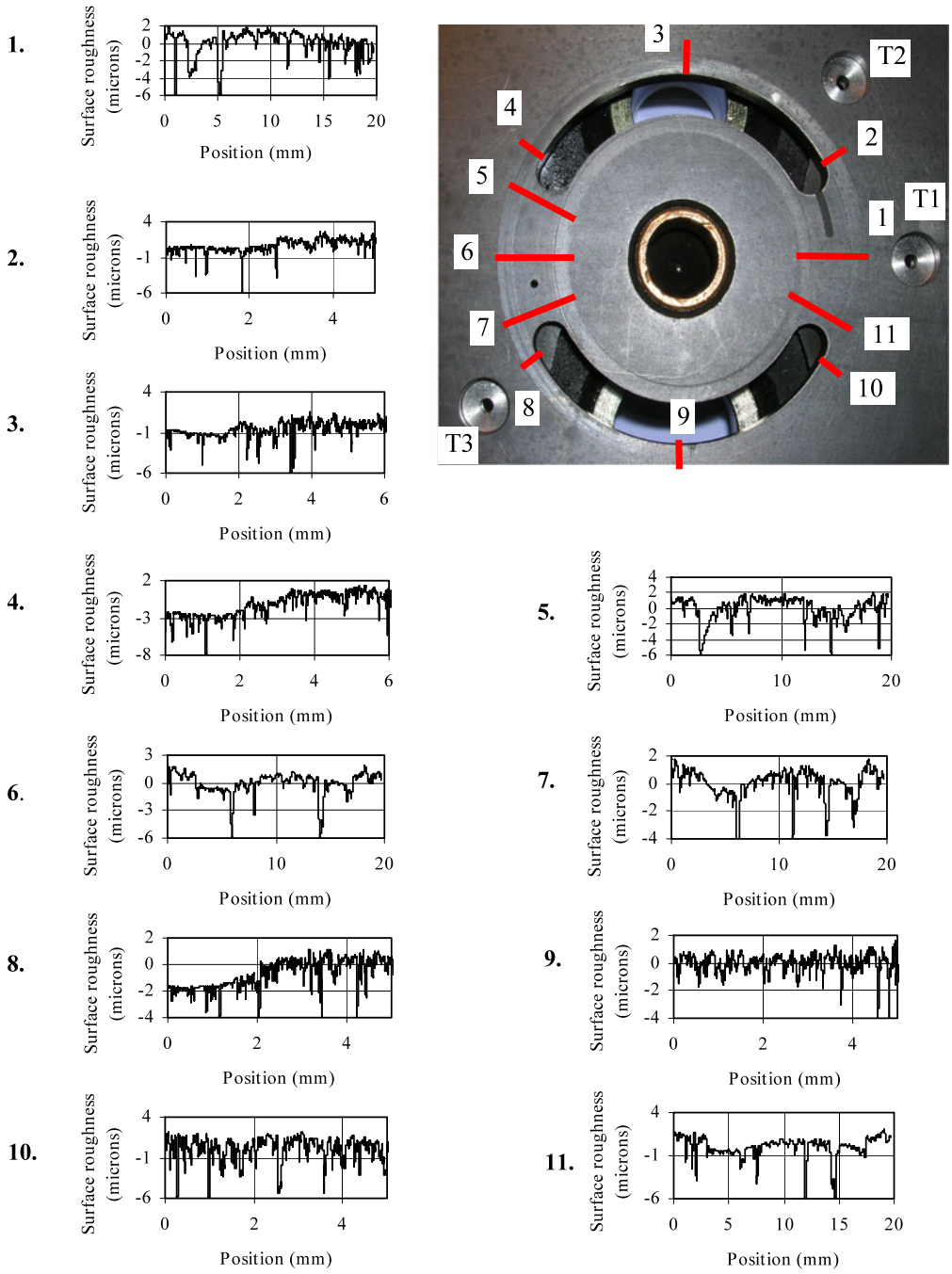

Fig. 4 Port plate face surface direct measurements

This indicates that the oil film thickness at this point is generally sufficient to prevent plastic metal-to-metal contact.

According to Fig. 6a the average film thickness dependency on swash plate angle is negligible at high temperatures. Figure 6b shows that at low pressures, low temperatures and low swash plate angles, transducer 3 is likely to give higher values than transducer 2, producing a shift in the position of the maximum film thickness, as it is reported in Fig. 7.

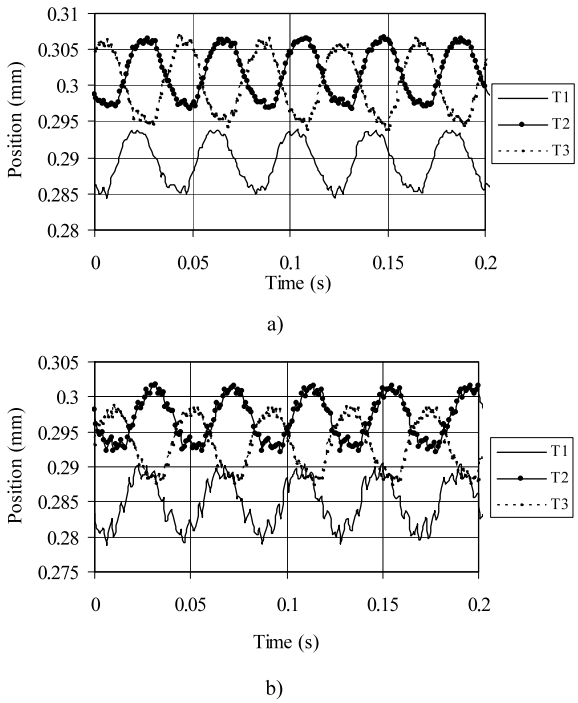

Fig. 5 Typical measured distance between the barrel plate aluminium disk and the port plate. Swash plate angle 20 degrees, 28°C (**a**) 2.5 MPa; (**b**) 17.5 MPa

It can be concluded that in general the film thickness around the pump outlet kidney port is higher than the film thickness around the tank kidney port. When oil temperature, swash plate angles and pressure are small, the film thickness maximum position suffers a small displacement versus its generic position.

If the average values of the three transducers are understood as the average clearance measured between the aluminium plate and the port plate internal face, and assuming the three points as belonging to a plane, the rest of the average points around the barrel can be calculated

The equation of a plane given three points takes the form, $aX + bY + cZ + d = 0$. Where the constants a, b, c and d, have to be calculated from the X, Y, Z position of the three given points, using (1).

$$\begin{bmatrix} x - x_1 & y - y_1 & z - z_1 \\ x - x_2 & y - y_2 & z - z_2 \\ x - x_3 & y - y_3 & z - z_3 \end{bmatrix} = 0; \tag{1}$$

where (x_1, y_1); (x_2, y_2); (x_3, y_3); are the three position points where the transducers are located, values presented in Sect. 2. The dimensions z_1, z_2, z_3, are the average distances between the port plate face and the barrel aluminium disk face, measured by the three transducers and presented in Fig. 6. The average position of any point in the same plane or in a parallel plane can easily be determined; therefore the location of the points where maximum and minimum average film thickness exists can be determined.

Figure 7 shows the general shape of the average film thickness at the barrel external land central diameter $2r_{mext}$, and for two different swash plate angles, 10° and 20°, two different oil temperatures, 28°C and 45°C and two pump output pressures, 2.5 and 12.5 MPa. It is necessary to consider that, port plate and barrel sliding surfaces are eroded, then, metal to metal contact will in fact appear for a film thickness of less than −4 μm, therefore, the values in Fig. 7 smaller than −4 μm, represents elastic and probably plastic metal to metal contact between the barrel face and the port plate surface. According to Fig. 7, just for high temperatures and high pressures, a very narrow area of the port plate will be in contact with the barrel and as it will be seen in Sect. 4, the elastic torque generated due to the contact is just a fraction of the pressure generated torque.

From Fig. 7, it is seen that at low pressures and low temperatures, the effect of the swash plate angle, slightly modifies the average film thickness. However as temperature increases, and/or pressure increases, the swash plate angle has no appreciable effect on the oil average film thickness. In both cases, at both low and high pressures, the predominant effect on the average film thickness variation is the oil temperature; as the fluid temperature increases, the film thickness decreases. Also when comparing Figs. 7a with b it is noticed that as pressure increases, the film thickness tends to slightly decrease. It must be pointed out that under some of the conditions studied, metal-to-metal contact exists and therefore mixed lubrication is often present. It needs to be considered that, according to Fig. 4 and due to the port plate erosion, the barrel can easily enter over 4 μm inside the port plate without having metal to metal contact. Mixed lubrication is more severe for high pressures and high oil temperatures. Figure 7 also shows, that the position of the maximum average film thickness for this particular pump is to be found at 120° clockwise versus the X^+ axis, see Fig. 1, and this maximum film thickness position remains constant for nearly all the test performed. At low pressures, low swash plate angles and low temperatures a shift in the average maximum film thickness

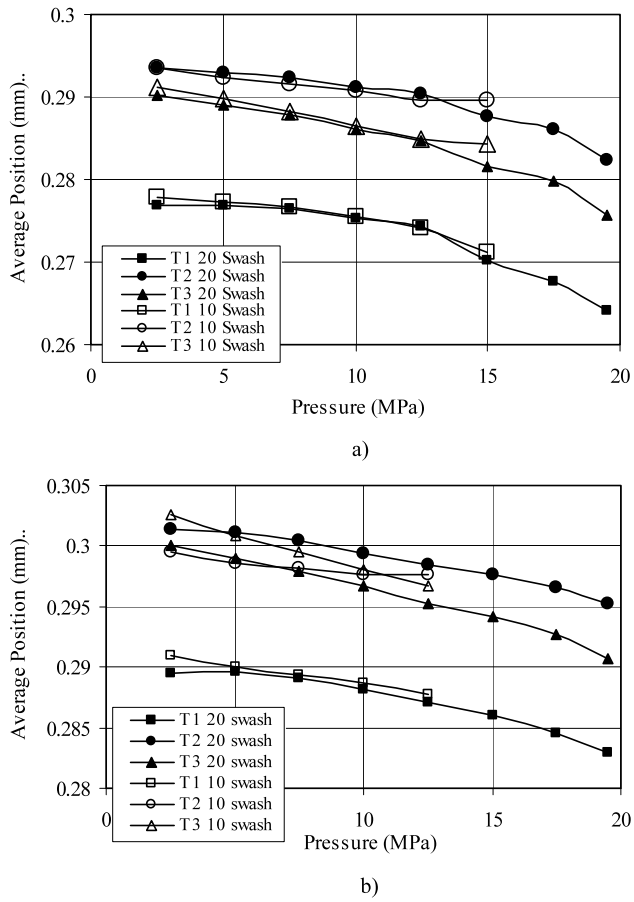

Fig. 6 Average measured transducers position for 10° and 20° swash plate angle. (**a**) Oil temperature 45°C. (**b**) Oil temperature 28°C

location is being encountered. For such cases the maximum position is found at 140° clockwise versus the X^+ axis, see Fig. 1d.

3.3 Barrel dynamics, fluctuation wave

Figure 8 shows the fluctuation wave superimposed on the sinusoidal main wave. These graphs have been obtained via subtracting the sinusoidal main waves due mostly to the disk runout, from the overall waves measured for each case. An example of such overall waves is to be found in Figs. 3 and 5. As already explained, the fluctuation wave measured by transducer 1 is much higher than the one measured by other transducers. This happens under all conditions studied.

From Fig. 8 transducer 1, it can be seen that at 5 MPa. The fluctuation is sharp and irregular, it can not be seen any pattern, its peak to peak amplitude is about 1.75 microns and the frequency oscillates between 190 and 1000 Hz.

At 15 MPa, transducer 1, the fluctuation shape has a clear pattern, which is similar to the theoretical one presented in [14], also Yamaguchi [11] found a similar trend. In fact, as pressure increases the experimental signal increases its similarity with the theoretical wave defined in [14]. There are three peaks appearing between the small and main peaks, its origin will be studied in the next section. The maximum amplitude found is around 3 microns, the frequencies range between 200 and 1100 Hz.

Transducer 2 follows the same trend as transducer 1, since it is located nearby; transducer 3 produces a more random frequency wave, then its location is on the opposite site of the port plate.

Although all graphs at different pressures are not presented in this paper, when studying the evolution of the fluctuation peaks with pressure, it is found that as

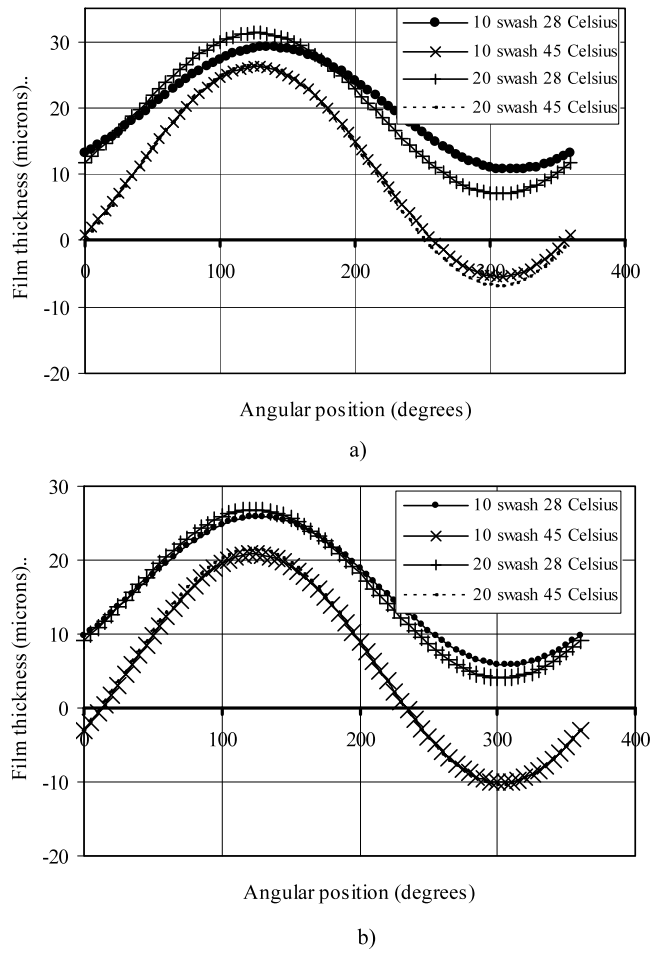

Fig. 7 Average calculated film thickness at two swash plate angles of 10° and 20°, oil temperatures, 28°C, 45°C, pressures, (**a**) 2.5 MPa, (**b**) 12.5 MPa

pressure increases the fluctuation wave amplitude increases, the decrease of oil temperature and or swash plate angle produces a decrease on the fluctuation wave amplitude, but the trend remains the same as the one presented in Fig. 8. Notice as well that in all cases studied, the minimum oscillation frequency appearing is about 200 Hz. A frequency of 216 Hz corresponds to the torque created by each piston when entering in contact with the timing groove and leaving the pressure kidney port, Bergada et al. [14]. This explains why transducer 1 is always giving a clearer pattern than the other two transducers, then transducer 1 is located nearby the timing groove. Under most of the conditions studied, and more especially at high pressures, a high frequency of around 1100 Hz appears and is believed to be due to the metal-to-metal contact between the barrel face and the port plate. In fact, this frequency is believed to be the number of metal to metal contacts the barrel face and the swash plate are having per second, as it will be clarified in the next section.

4 Barrel dynamics

The fundamental independent dynamic equations over the X and Y barrel axes were derived in [14]. Such equations relate the input torques M_X; M_Y; due to the pressure distribution acting over the barrel to the barrel inertia, damping coefficient, spring constant and barrel/port plate friction. However, as shown in Fig. 4, the port plate suffers elastic and plastic deformation.

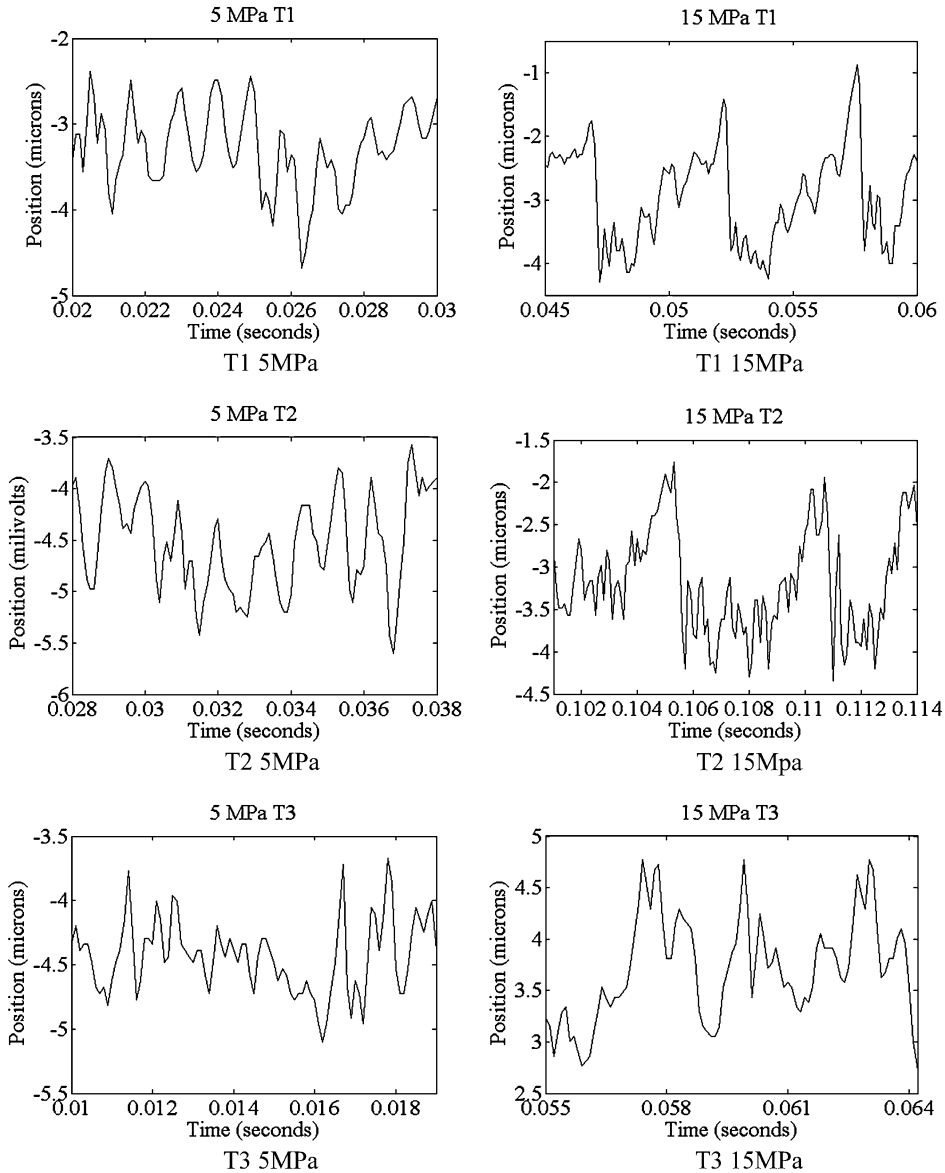

Fig. 8 Position fluctuation from transducers 1, 2, 3. 5, 15 MPa, oil temperature 45°C, 20° swash plate angle

Therefore, in order to consider metal-to-metal elastic torque, which constant is M_E, a new term has been included in the previous barrel dynamic model, the barrel modified dynamic equations are summarised as (2), (3).

$$I_x\ddot{\delta} + B_x\dot{\delta} + K_x(\delta - \delta_0) + F_{forces_x} \cdot \operatorname{sign}(\dot{\delta}) + \overbrace{\frac{EA_0}{L_0}r^2}^{M_E} \max(|\delta| - \delta_L; 0) = M_X \tag{2}$$

$$I_y\ddot{\eta} + B_y\dot{\eta} + K_y(\eta - \eta_0) + F_{forces_y} \cdot \operatorname{sign}(\dot{\eta}) + \overbrace{\frac{EA_0}{L_0}r^2}^{M_E} \max(|\eta| - \eta_L; 0) = M_Y \tag{3}$$

To develop the metal to metal elastic torque, the following procedure has been used.

The force F exerted by the material when compressed or stretched by ΔL and as a function of the

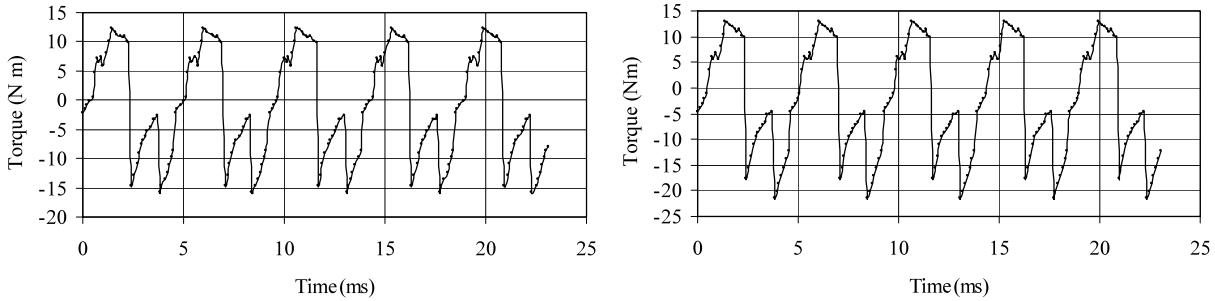

Fig. 9 Calculated input torques M_X, pump output pressures (**a**) 15 MPa, (**b**) 17.5 MPa

original length L_0, contact area A_0 and the bulk modulus E is:

$$F = \frac{EA_0\Delta L}{L_0} \tag{4}$$

The distance the barrel enters into the port plate can be given as: $\Delta L = r\delta$. Taking into account that metal to metal contact appears just when the tilt is higher than the maximum angular value in which still does not exist metal to metal contact δ_L, then:

$$\Delta L = r(|\delta| - \delta_L) \tag{5}$$

$|\delta|$ is the angular value calculated with simulink, the absolute value considers that metal to metal contact can exist in both axis directions. If the angular distance displaced by the barrel is smaller than δ_L, there will not exist metal to metal contact, and this is expressed as:

$$\Delta L = r\max(|\delta| - \delta_L; 0) \tag{6}$$

Finally, the torque created by the elastic forces will be:

$$M_{EF} = \frac{EA_0}{L_0} r^2 \max(|\delta| - \delta_L; 0) \tag{7}$$

The damping coefficient for the barrel piston assembly may be considered small, but it is highly dependent on oil temperature. Elastic metal to metal forces exist between the barrel face and the port plate; they act in opposite direction than the input torque and depend on the Young modulus, the area of contact and the distance the barrel penetrates into the plate. Although such elastic forces can in general be considered small when studying the barrel X, Y axis acceleration, they play a relevant role regarding the barrel dynamics.

The torsional spring constant created by the pump axis and spring, although difficult to accurately determine, has to play an important role when studying the barrel dynamics, the spring located at the bottom of the barrel, for this particular pump is 22.5 mm long, being its constant of 134.8 N/mm. Inertia effects will also need to be considered. Since the moment of inertia changes as the barrel rotates, the barrel plus pistons moment of inertia will be time dependent, although negligible in this example. The peak to peak variation is around 0.5% of the mean values $I_x = I_y = 0.0127\ \text{kg m}^2$. The input torques, M_X, M_Y, were developed in [14] and the M_X equations for the main pressure groove and the timing groove are presented in Appendix. These torques act as inputs and are generated as data files to allow a dynamic solution via the MATLAB Simulink package.

Since this section is focused on understanding the origin of the barrel high frequency fluctuations, just the dominant fluctuation torque about the Y axis will be considered. Then as previously explained, the origin of the fluctuation wave is to be found along the X axis. Figure 9 presents three input perturbation torques using equations (A.1), (A.2) M_X, generated along the X axis, for two different pump output pressures, 15 and 17.5 MPa. The process of calculation of this torque was fully explained in [14] and due to its complexity shall not be repeated here. Introducing these torques as inputs, several dynamic barrel fluctuations as a function of the damping coefficient B, spring torsional constant K and the elastic metal-to-metal reaction torque constant M_E were found and presented in Fig. 10. Despite the fact that for the present simulation, the metal-to-metal friction torque has been considered negligible, since the objective was to study the

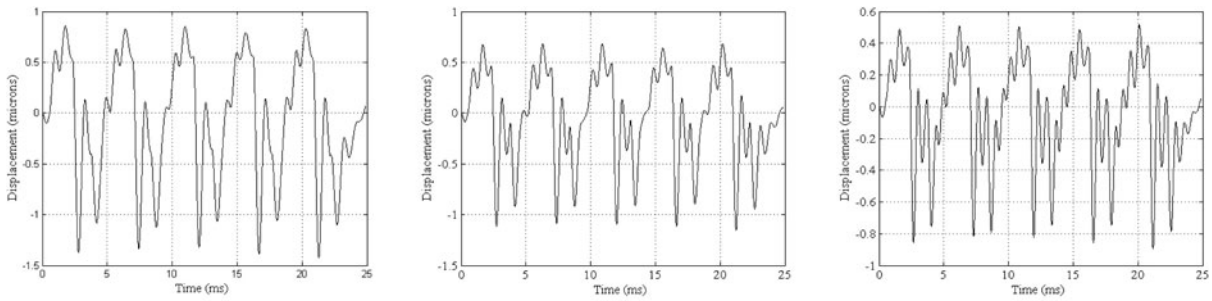

(a) 15 MPa, $K = 6 \times 10^5$ Nm, $B = 35$ Nm s/rad, $M_E = 0$ Nm
(b) 15 MPa, $K = 6 \times 10^5$ Nm, $B = 35$ Nm s/rad, $M_E = 1.68 \times 10^5$ Nm
(c) 15 MPa, $K = 6 \times 10^5$ Nm, $B = 35$ Nm s/rad, $M_E = 5.6 \times 10^5$ Nm

Fig. 10 Fluctuation wave simulation results

effect of elastic forces, it has been found that the inclusion of such torque produces a similar effect than the elastic torque. Both enhance the fluctuation wave peaks amplitude. From these results it is noticed that if the spring torsional constant is big enough, the barrel will be able to follow the input torque generated by the pump. In fact, the metal-to-metal elastic forces play a decisive role when studding the barrel dynamics, as it is seen from Figs. 10a, b, c. Notice that, the simulated results shown in Fig. 10, resembles very closely the experimental ones presented in Fig. 8. It is therefore demonstrated that the frequencies of around 1100 Hz, are in fact appearing when the pump barrel has a very high stiffness, and able to follow the small torque perturbations created by the pump along the X axis. Such large stiffness appears at high pressures and high temperatures showing that under these conditions the barrel response is very fast. It is demonstrated that when the elastic torque is considered, the fluctuation peaks amplitude increase, Fig. 10b, c, clearly showing that elastic metal to metal forces need to be considered when aiming to understand the full barrel dynamics. In reality, elastic barrel/port plate forces can be quite different in time, since the metal-to-metal forces depend on the random contact between surfaces. This explains why the measured frequencies of the fluctuation peaks are not constant, although vary around 1100 Hz.

5 Conclusions

Barrel/port plate average film thickness and barrel dynamics have been experimentally evaluated for a range of operating conditions.

Average film thickness decreases mostly with the increase of the oil temperature, and has a smaller decrease with the increase of pump outlet pressure. Therefore at low pressures and low temperatures the average film thickness is at its maximum. As pressure and temperature increases, film thickness decreases, and mixed lubrication it is expected in most of the barrel/port plate surface. The barrel then undergoes a wobbling motion.

The swash plate angle variation has a small effect on the average film thickness; nevertheless it has been found that at small swash plate angles, the average film thickness slightly increases.

The average film thickness around the pump outlet kidney port is thicker than the film thickness around the tank kidney port for nearly all conditions studied. The maximum film thickness for this particular pump is located around 120 degrees anticlockwise from the (X^+) axis for most of the cases studied.

Due to the barrel aluminium measuring plate run-out, the position measured by the transducers presents a sinusoidal-type variation with a frequency of 24 Hz. In addition, a fluctuating component was found to be sitting onto the main wave. The displacement fluctuating wave has two main peaks, a small one related to the torque created when each piston enters in contact with the timing groove, and a main one created when each piston leaves the pressure kidney port. This occurs at a frequency of 216 Hz, that is, pump speed multiplied by the number of pistons. Along with the main fluctuation component, a second component occurs at a frequency around 1000–1100 Hz. This second component is more clearly seen when the system stiff-

ness is high, system stiffness depending on the pump spring constant, pump central axis constant, and elastic/plastic metal-to-metal reaction forces.

As pressure increases, film thickness decreases, metal-to-metal contact increases and the fluctuating wave small perturbation peaks are more evident. The damping coefficient plays an important role regarding the barrel dynamics since as temperature increases, the damping coefficient decreases, allowing the barrel to move more freely. This is why at high temperatures and high pressures the fluctuation wave is more clearly seen. The elastic/plastic metal-to-metal forces, enhances the fluctuating wave peaks increasing their amplitude.

Appendix

The fluid-derived M_X torque generated by the pressure distribution between the barrel and port plate are derived in detail in [14]. The resulting equations are as follows:

(i) due to the main groove (pressure groove).

$$
\begin{aligned}
M_X = {} & \int_{-\theta_i}^{\theta_j} \frac{3\mu\omega\alpha r_{mint}\sin^2\theta d\theta}{(h_0+\alpha r_{mint}\cos\theta)^3} \\
& \times\left[\frac{r_{int}^2}{6}\left(r_{int}^3-r_{int2}^3\right)-\frac{(r_{int}^5-r_{int2}^5)}{10}\right. \\
& +\frac{(r_{int2}^2-r_{int}^2)}{6}\left(r_{int}^3-r_{int2}^3\right)\frac{\ln(r_{int})}{\ln(\frac{r_{int}}{r_{int2}})} \\
& -\frac{(r_{int2}^2-r_{int}^2)}{2\ln(\frac{r_{int}}{r_{int2}})} \\
& \times\left[\frac{(r_{int2}^3-r_{int}^3)}{9}\right. \\
& \left.\left.+\frac{r_{int}^3\ln(r_{int})-r_{int2}^3\ln(r_{int2})}{3}\right]\right] \\
& +\int_{-\theta_i}^{\theta_j} \frac{3\mu\omega\alpha r_{mext}\sin^2\theta d\theta}{(h_0+\alpha r_{mext}\cos\theta)^3} \\
& \times\left[\frac{r_{ext}^2}{6}(r_{ext2}^3-r_{ext}^3)-\frac{(r_{ext2}^5-r_{ext}^5)}{10}\right. \\
& +\frac{(r_{ext2}^2-r_{ext}^2)}{6}(r_{ext2}^3-r_{ext}^3)\frac{\ln(r_{ext})}{(\frac{r_{ext}}{r_{ext2}})} \\
& -\frac{(r_{ext2}^2-r_{ext}^2)}{2(\frac{r_{ext}}{r_{ext2}})}\left[\frac{(r_{ext}^3-r_{ext2}^3)}{9}\right. \\
& \left.\left.\left.+\frac{r_{ext2}^3\ln(r_{ext2})-r_{ext}^3\ln(r_{ext})}{3}\right]\right] \qquad \text{(A.1)}
\end{aligned}
$$

(ii) due to the timing groove

$$
\begin{aligned}
M_{X_{sg}} = {} & \frac{p_{ext}}{3}(r_{ext2}^3-r_{int2}^3)[-\cos\theta]_{-(\theta_i+\gamma)}^{-\theta_i} \\
& +\frac{(p_{int}-p_{ext})}{9}\left[\frac{r_{int2}^3-R_{int}^3}{\ln(\frac{R_{int}}{r_{int2}})}\right. \\
& \left.+\frac{R_{ext}^3-r_{ext2}^3}{\ln(\frac{R_{ext}}{r_{ext2}})}\right] \\
& \times[-\cos\theta]_{-(\theta_i+\gamma)}^{-\theta_i} \\
& +\int_{-(\theta_i+\gamma)}^{-\theta_i}\frac{3\mu\omega\alpha R_{mint}\sin^2\theta d\theta}{(h_0+\alpha R_{mint}\cos\theta)^3} \\
& \times\left[\frac{(R_{int}^5-r_{int2}^5)}{15}\right. \\
& \left.-\frac{(r_{int2}^2-R_{int}^2)}{18}\frac{(r_{int2}^3-R_{int}^3)}{\ln(\frac{R_{int}}{r_{int2}})}\right] \\
& +\int_{-(\theta_i+\gamma)}^{-\theta_i}\frac{3\mu\omega\alpha R_{mext}\sin^2\theta d\theta}{(h_0+\alpha R_{mext}\cos\theta)^3} \\
& \times\left[\frac{(r_{ext2}^5-R_{ext}^5)}{15}\right. \\
& \left.-\frac{(r_{ext2}^2-R_{ext}^2)}{18}\frac{(R_{ext}^3-r_{ext2}^3)}{\ln(\frac{R_{ext}}{r_{ext2}})}\right] \qquad \text{(A.2)}
\end{aligned}
$$

The independent mechanical dynamic equation over the X barrel axis, presented in Sect. 4, has as input the calculated torque M_X given by the equations just introduced.

References

1. Helgestad BO, Foster K, Bannister FK (1974) Pressure transients in an axial piston hydraulic pump. Proc Inst Mech Eng 188(17/74):189–199
2. Martin MJ, Taylor B (1978) Optimised port plate timing for an axial piston pump. In: 5th int fluid power symposium, Cranfield, England, 13–15 September 1978, vol B5, pp 51–66
3. Edge KA, Darling J (1989) The pumping dynamics of swash plate piston pumps. J Dyn Syst Meas Control 111:307–312

4. Mandal NP, Saha R, Sanyal D (2008) Theoretical simulation of ripples for different leading-side groove volumes on manifolds in fixed-displacement axial-piston pump. Proc Inst Mech Eng, Part I, J Syst Control Eng 222:557–570
5. Yamaguchi A (1987) Formation of a fluid film between a valve plate and a cylinder block of piston pumps and motors (2nd report, a valve plate with hydrostatic pads). JSME Int J 30(259):87–92
6. Manring ND (2003) Valve-plate design for an Axial Piston pump operating at low displacements. ASME J Mech Eng 125:200–205
7. Johansson A (2005) Design principles for noise reduction in hydraulic piston pumps—simulation, optimisation and experimental verification. PhD thesis, Linkoping University
8. Seeniraj GK, Ivantysynova M (2006) Impact of valve plate design on noise, volumetric efficiency and control effort in an axial piston pump. In: Proceedings of ASME international mechanical engineering congress and exposition, IMECE2006, Chicago, IL, USA
9. Seeniraj GK, Ivantysynova M (2008) Multi-objective optimization tool for noise reduction in axial piston machines. SAE Int J Commer Veh 1(1):544–552
10. Seeniraj G (2009) Model based optimization of axial piston machines focusing on noise and efficiency. PhD thesis, Purdue University
11. Yamaguchi A (1990) Bearing/seal characteristics of the film between a valve plate and a cylinder block of axial piston pumps: Effects of fluid types and theoretical discussion. J Fluid Control 20(4):7–29
12. Matsumoto K, Ikeya M (1991) Friction and leakage characteristics between the valve plate and cylinder for starting and low speed conditions in a swashplate type axial piston motor. Trans Jpn Soc Mech Eng C 57:2023–2028
13. Matsumoto K, Ikeya M (1991) Leakage characteristics between the valve plate and cylinder for low speed conditions in a swashplate-type axial piston motor. Trans Jpn Soc Mech Eng C 57:3008–3012
14. Bergada JM, Watton J, Kumar S (2008) Pressure, flow force and torque between the barrel and port plate in an axial piston pump. J Dyn Syst Meas Control 130(1):011011-1/16
15. Jacazio G, Vatta F (1981) The block-lift in axial piston hydraulic motors. In: The ASME/ASCE bioengineering, fluids engineering and applied mechanics conference, Boulder, Colorado USA, 22–24 June 1981, pp 1–7
16. Kobayashi S, Matsumoto K (1993) Lubrication between the valve plate and cylinder block for low speed conditions in a swashplate-type axial piston motor. Trans Jpn Soc Mech Eng C 59:182–187
17. Weidong G, Zhanlin W (1996) Analysis for the real flow rate of a swash plate axial piston pump. J Beijing Univ Aeronaut Astronaut 22(2):223–227
18. Yamaguchi A (1997) Tribology of hydraulic pumps. ASTM Spec Tech Publ 1310:49–61
19. Yamaguchi A, Sekine H, Shimizu S, Ishida S (1987) Bearing/seal characteristics of the Oil film between a valve plate and a cylinder block of axial pumps. JHPS 18(7):543–550
20. Manring ND (2000) Tipping the cylinder block of an axial-piston swash-plate type hydrostatic machine. J Dyn Syst Meas Control 122:216–221
21. Ivantysynova M, Grabbel J, Ossyra JC (2002) Prediction of swash plate moment using the simulation tool CASPAR. In: Proceedings of IMECE 2002 ASME international mechanical engineering congress & exposition IMECE2002-39322, New Orleans, LA USA, 17–22 November 2002, pp 1–9
22. Ivantysynova M, Huang C (2002) Investigation of the flow in displacement machines considering elastohydrodynamic effect. In: Proceedings of the 5th JFPS international symposium on fluid power, Nara, Japan, vol 1, pp 219–229
23. Ivantysynova M (1999) A new approach to the design of sealing and bearing gaps of displacement machines. In: Fluid power forth JHPS international symposium, pp 45–50
24. Ivantysynova M, Baker J (2009) Power loss in the lubricating gap between cylinder block and valve plate of swash plate type axial piston machines. Int J Fluid Power 10(2):29–43
25. Jouini N, Ivantysynova M (2008) Valve plate surface temperature prediction in axial piston machines. In: Proc. of the 5th FPNI PhD symposium, Cracow, Poland, pp 95–110
26. Baker J, Ivantysynova M (2008) Investigation of power losses in the lubricating gap between the cylinder block and valve plate of axial piston machines. In: Proc. of the 5th FPNI PhD symposium, Cracow, Poland, pp 302–319. Best paper award
27. Ivantysynova M (2008) Innovations in pump design—what are future directions? In: Proceedings of the 7th JFPS international symposium on fluid power, Toyama, pp 59–64. Invited lecture organized session agriculture and mining machinery
28. Pelosi M, Zecchi M, Ivantysynova M (2010) A fully coupled thermo-elastic model for the rotating kit of axial piston machines. In: ASME/Bath international symposium on fluid power and motion control (FPMC2010), pp 217–234
29. Baker J, Ivantysynova M (2009) Advanced surface design for reducing power losses in axial piston machines. In: Proceedings 11th Scandinavian international conference on fluid power, SICFP'09, Linköping, Sweden, 2–4 June 2009
30. Pelosi M, Ivantysynova M (2009) A novel fluid-structure interaction model for lubricating gaps of piston machines. In: Brebbia CA (ed) Proceedings of the fifth fluid structure interaction conference. WIT Press, Southampton, pp 13–24
31. Zeiger G, Akers A (1985) Torque on the swashplate of an axial piston pump. J Dyn Syst Meas Control 107:220–226
32. Zeiger G, Akers A (1986) Dynamic analysis of an axial piston pump swashplate control. Proc Inst Mech Eng 200(C1):49–58
33. Inoue K, Nakasato M (1994) Study of the operating moment of a swash plate type axial piston pump First report, effects of dynamic characteristics of a swash plate angle supporting element on the operating moment. J Fluid Control 22(1):30–46
34. Inoue K, Nakasato M (1994) Study of the operating moment of a swash plate type axial piston pump Second report, effects of dynamic characteristics of a swash plate angle supporting element on the cylinder pressure. J Fluid Control 22(1):7–29
35. Manring ND, Johnson RE (1996) Modeling and designing a variable-displacement open-loop pump. J Dyn Syst Meas Control 118:267–271
36. Wicke Edge KA V, Vaughan D (1998) Investigation of the effects of swash plate angle and suction timing on the noise

generation potential of an axial piston pump. Fluid Power Syst Technol 5:77–82
37. Ivantysynova M, Lasaar R (2004) An investigation into micro- and macrogeometric design of piston/cylinder assembly of swash plate machines. Int J Fluid Power 5(1):23–36
38. Manring ND (1999) The control and containment forces on the swash plate of an axial piston pump. J Dyn Syst Meas Control 121:599–605
39. Gilardino L, Mancò S, Nervegna N, Viotto F (1999) An experience in simulation the case of a variable displacement axial piston pump. In: Forth JHPS international symposium, pp 85–91, paper 109
40. Manring ND (2002) The control and containment forces on the swash plate of an axial piston pump utilizing a secondary swash-plate angle. In: Proceedings of the American control conference, Anchorage, AK, USA, 8–10 May 2002, pp 4837–4842
41. Manring ND (2002) Designing a control and containment device for a cradle-mounted, axial-actuated swash plates. J Mech Des 124:456–464
42. Bahr MK, Svoboda J, Bhat RB (2003) Vibration analysis of constant power regulated swash plate axial piston pumps. J Sound Vib 259(5):1225–1236
43. Metha V (2006) Torque ripple attenuation for an axial piston swash plate type hydrostatic pump, noise considerations. PhD thesis, Missouri University
44. Hong YS, Lee SY (2008) A comparative study of Cr-X-N (X = Zr, Si) coatings for the improvement of the low speed torque efficiency of a hydraulic piston pump. Met Mater Int 14(1):33–40
45. Hong YS, Lee SY, Kim SH, Lim HS (2006) Improvement of the low-speed friction characteristics of a hydraulic piston pump by PVD-coating of TiN. J Mech Sci Technol 20(3):358–365